LETTER

doi:10.1038/nature18639

Electron attraction mediated by Coulomb repulsion

A. Hamo[1]*, A. Benyamini[1]*, I. Shapir[1]*, I. Khivrich[1], J. Waissman[1]†, K. Kaasbjerg[1]†, Y. Oreg[1], F. von Oppen[2] & S. Ilani[1]

One of the defining properties of electrons is their mutual Coulomb repulsion. However, in solids this basic property may change; for example, in superconductors, the coupling of electrons to lattice vibrations makes the electrons attract one another, leading to the formation of bound pairs. Fifty years ago it was proposed[1] that electrons can be made attractive even when all of the degrees of freedom in the solid are electronic, by exploiting their repulsion from other electrons. This attraction mechanism, termed 'excitonic', promised to achieve stronger and more exotic superconductivity[2–6]. Yet, despite an extensive search[7], experimental evidence for excitonic attraction has yet to be found. Here we demonstrate this attraction by constructing, from the bottom up, the fundamental building block[8] of the excitonic mechanism. Our experiments are based on quantum devices made from pristine carbon nanotubes, combined with cryogenic precision manipulation. Using this platform, we demonstrate that two electrons can be made to attract each other using an independent electronic system as the 'glue' that mediates attraction. Owing to its tunability, our system offers insights into the underlying physics, such as the dependence of the emergent attraction on the underlying repulsion, and the origin of the pairing energy. We also demonstrate transport signatures of excitonic pairing. This experimental demonstration of excitonic pairing paves the way for the design of exotic states of matter.

Following the development of the Bardeen–Cooper–Schrieffer (BCS) theory of superconductivity[9], W. A. Little[1] proposed the idea that two electrons can attract each other not via phononic-based attraction, but via their repulsion from other electrons. He predicted that if electrons, which are much lighter than ions, mediate the attraction, then the electron pairing would be much stronger than in conventional superconductors. To test this new form of attraction, Little proposed a one-dimensional conducting organic chain (Fig. 1a, green) that has an array of polarizable sidechains ('polarizers', purple). Each polarizer has a single electron that can hop between two sites—one closer to and one further away from the main chain. Owing to Coulomb repulsion, an electron travelling down the main chain polarizes the side chains, which in turn attracts another electron in the main chain. This mechanism rapidly became popular in attempts to engineer unconventional superconductivity; it was extended to two dimensions[2,3], generalized to attraction at localized sites[10–14] and used in early attempts to explain high-T_c superconductivity[15]. It is considered a candidate for the unusual superconductivity[16,17] and pairing[18] observed in $SrTiO_3$ interfaces, and it has analogues in optical systems[19]. Numerous attempts have been made to directly synthesize organic materials that have the essential microscopic components[7]; however, so far there has not been any experimental evidence for an excitonic attraction between electrons.

At the core of Little's proposal is the idea that electrons separate into two groups: some form the 'system' (Fig. 1a, green), where their mutual interaction is to become attractive, while others make up the surrounding 'medium' (purple) that produces the 'glue' for the attraction. To make electrons attractive, this medium should perform the unusual feat of flipping the sign of the potential generated by the system electrons, making them look like holes to other system electrons (Fig. 1b). This suggests that the medium should effectively have a negative dielectric constant. Little suggested that this property can be achieved in the dynamic (retarded) limit, in which the system electrons respond faster than the medium, thus leaving a positive polarization cloud in their wake that creates an exponentially weak BCS-like pairing. However, Hirsch and Scalapino showed[5] that the interesting regime of Little's model is instead the static (instantaneous) limit. Only in that limit does superconductivity dominate over competing orders (such as charge and spin density waves) and the superconducting phase exhibit strong Bose–Einstein-condensation-like pairing.

Here we demonstrate that excitonic pairing is indeed possible and that the key ingredient is the discreteness of the electrons in the medium. We take a bottom-up approach and construct the minimal building block of Little's model that features excitonic attraction[8]—a two-site system and a single polarizer (Fig. 1a, dashed circle)—and show that when the polarizer interacts strongly with the system, it can render its electrons attractive.

The system and polarizer are created within two separate carbon nanotubes, each on its own microchip. We use our recently developed nano-assembly technique[20] to suspend each nanotube between two metallic contacts and above an array of gates (Supplementary Information section S1). In both devices we bias the gates to produce a double-well electrostatic potential along the nanotube length (Fig. 1c). In the polarizer device, the energy levels in the two wells are placed far from the chemical potential in the leads, but close to each other, such that a single electron can hop between the wells, but cannot escape to the leads. The polarizer thus operates as an isolated dipole whose sole degree of freedom is the polarization of its electron (Supplementary Information section S2). Conversely, in the system device, a large central barrier inhibits tunnelling between the two wells, but small side barriers allow electrons to enter from their corresponding leads. On a separately contacted side segment of the system nanotube, we create an independent quantum dot that serves as a charge detector, detecting the population of individual system electrons via weak electrostatic coupling. We then mount the two chips, oppositely facing and perpendicular to each other, in a custom-built scanning probe microscope inside a dilution refrigerator (Fig. 1d). The microscope allows us to control the distance and the coupling between the polarizer nanotube and the system nanotube (Fig. 1d inset) and, hence, to test whether the polarizer alters the behaviour of the system electrons in a fundamental way.

We first measure the charge stability diagram of the bare system, without the polarizer. Using the left and right gates of the system, we scan the potential detuning between the two wells, $\delta V = (V_L - V_R)/2$, and their mean potential, $V = (V_L + V_R)/2$. Changes in the electronic occupation of the system appear as steps in the charge-detector current, I_{CD} (Supplementary Information section S2). This measurement (Fig. 2a) yields the well-known charge stability diagram of a double

[1]Department of Condensed Matter Physics, Weizmann Institute of Science, Rehovot 76100, Israel. [2]Dahlem Center for Complex Quantum Systems and Fachbereich Physik, Freie Universität Berlin, 14195 Berlin, Germany. †Present addresses: Department of Physics, Harvard University, Cambridge, Massachusetts 02138, USA (J.W.); Department of Micro- and Nanotechnology, Technical University of Denmark, DK-2800 Kongens Lyngby, Denmark (K.K.).
*These authors contributed equally to this work.

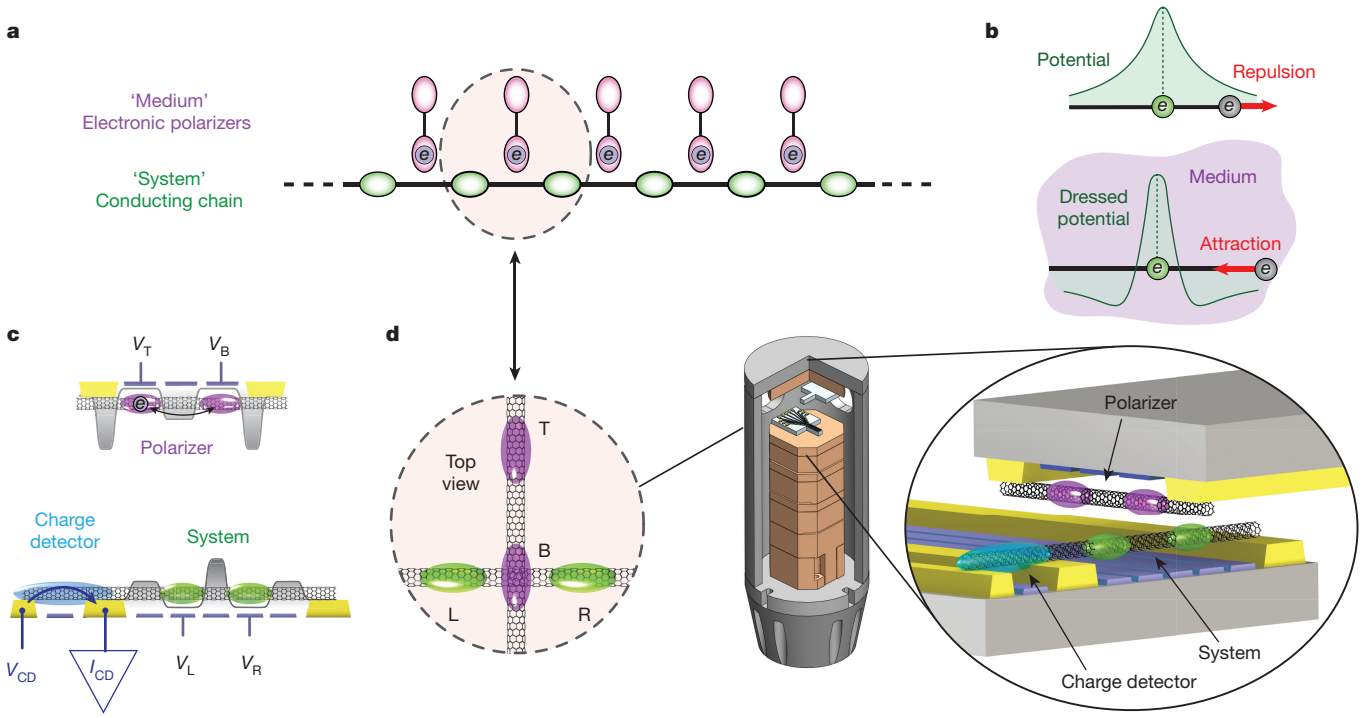

Figure 1 | Model system and experimental realization of its fundamental building block. a, The organic-molecule model system proposed by Little[1], consisting of two parts: the 'system', a one-dimensional conducting chain (individual lattice sites marked in green), and the 'medium', an array of side-chain 'polarizers' (purple) each having a single electron that can hop between a site close to, and a site further away from, the chain. The fundamental unit block that manifests attraction is a two-site system with one polarizer (dashed circle). **b**, In a bare electronic system (top) an electron creates a repulsive Coulomb potential (green). Embedding it in a medium that flips the sign of its potential (bottom) will make this electron attractive to other electrons. **c**, Implementation of the two components ('polarizer' and 'system') that make up the fundamental building block. These are fabricated as two separate devices, each having a pristine nanotube assembled on contacts (yellow) and suspended above an array of gates (blue), which set the potential landscape for the electrons (grey) (see Supplementary Information section S1 for dimensions). The polarizer device (top) has two gate voltages, V_B and V_T, that control the potentials of the bottom and top dots (purple), and is operated as an isolated dipole, whose sole degree of freedom is that of a single electron hopping between the sites. The system device (bottom) has two gate voltages, V_L and V_R, that control the potentials of the right and left dots (green). Here the central barrier is opaque and the side barriers are relatively transparent such that electrons enter the two dots from their corresponding leads. An additional dot on a side segment of the same nanotube (blue) serves as a single electron transistor charge detector: a voltage bias across it, V_{CD}, leads to current, I_{CD}, that is sensitive to the population of the system dots through weak electrostatic coupling. **d**, A custom-built scanning probe microscope (centre), operating inside a dilution refrigerator, brings the two oppositely facing devices into proximity (about 100–150 nm apart) such that the polarizer nanotube is perpendicular to the system nanotube (right) and such that one of its dots is directly above the system while the other is further away (left), creating a structure that is analogous to that of Little's molecule.

quantum dot with repulsive electrons (explained in Supplementary Information section S3). Tilted charging lines reflect the addition of a single electron to the right or left dot. Near their crossing, the charging lines exhibit a vertical shift (Fig. 2a, dashed black line), reflecting the fact that if one dot is occupied the energy to populate the other dot is increased by the Coulomb repulsion between the neighbouring electrons. This vertical shift is thus a direct fingerprint of the nearest-neighbour electron repulsion, and its magnitude normalized to energy units yields the strength of this repulsion, $W = 830\,\mu\text{eV}$.

Fundamentally different behaviour is observed when the polarizer is brought into close proximity to the system. In this case, we measure a charge stability diagram with an interaction line that is rotated from vertical to horizontal (Fig. 2b). This rotation implies that the polarizer inverts the interaction between the system electrons from repulsive to attractive. The inversion is best understood by realizing that the ground states at the centre of the two charge stability diagrams are fundamentally different: in the bare system it is a degenerate state between having a single electron on the left or the right dot (labelled (1, 0) and (0, 1)); with the polarizer nearby it becomes a paired ground state having a degeneracy between the two states with an even electron number (labelled (0, 0) and (1, 1)). The odd states, (1, 0) and (0, 1), become excited states, separated from the ground state by a pairing gap Δ. This gap is maximal at the centre of the horizontal vertex, where its magnitude is given by the length of this vertex (2Δ after normalization; see Supplementary Information section S4), reaching $\Delta = 790\,\mu\text{eV} \approx 8\,\text{K}$.

A medium can transform repulsive system electrons to attractive electrons only if it can flip the sign of the electrostatic potential produced by these electrons. The Coulomb potential of a bare electron is positive in its local and neighbouring sites, implying on-site and nearest-neighbour repulsion (Fig. 2c). If the on-site repulsion is retained while flipping the potential sign at the nearest-neighbour site, then the system remains stable, but acquires nearest-neighbour attraction. However, any medium based on continuum classical electrostatics can at best screen a potential to zero, but cannot flip its sign (Fig. 2d). We therefore seek to understand what the special feature of our polarizer medium is that enables such sign inversion.

The key element for a sign-inverting medium is charge discreteness[21] and, more fundamentally, the fact that a single electron does not repel itself. To understand this, compare the screening by a single-electron dipole to that of a metallic object of similar geometry (Fig. 2e). In a small external field, the charge in the metal will polarize slightly to exactly null the internal field. Conversely, in a dipole with small inter-site tunnelling, an entire electron will polarize between the two sites, creating an internal field that is much larger than, and of opposite sign to, the external field. This behaviour is the basis for our basic 'sign-inverter'. Unlike continuous charge in a metal that experiences its own field and thus minimizes the electrostatic energy by nulling the internal

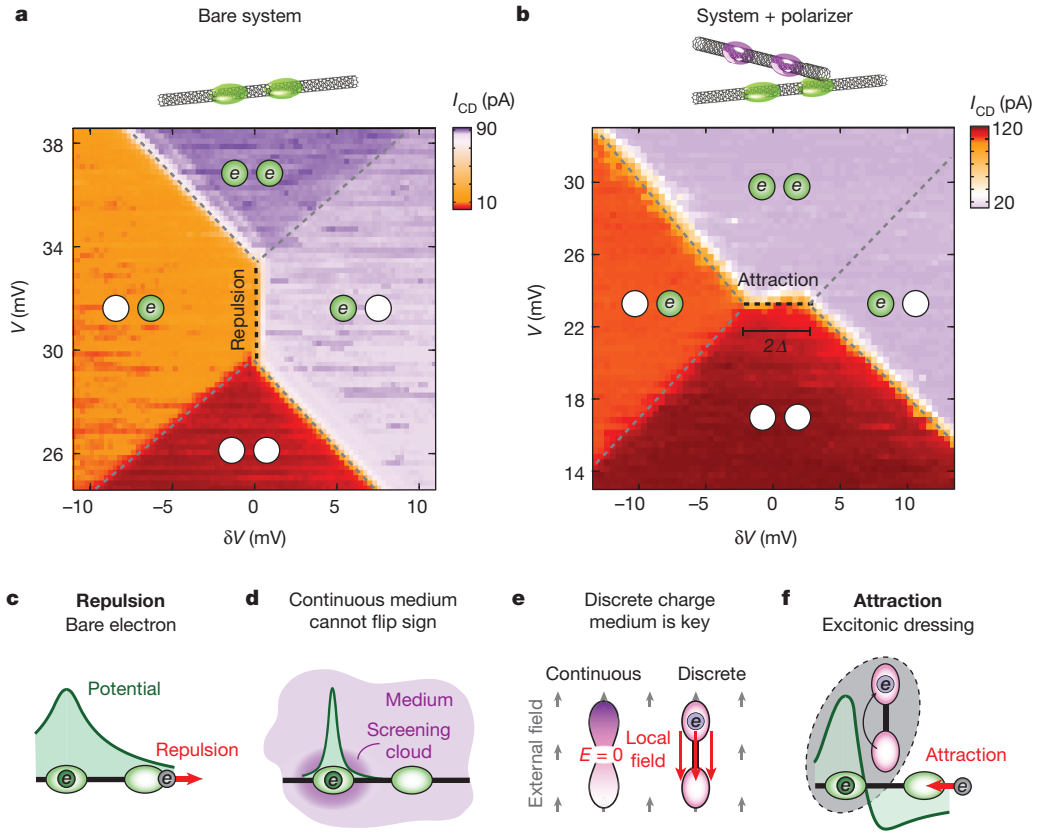

Figure 2 | From repulsive to attractive electrons. a, Measured charge stability diagram of the bare system: charge detector current (I_{CD}, colour scale) plotted as a function of the voltage detuning between its right (R) and left (L) sites, $\delta V = (V_L - V_R)/2$, and the mean gate voltage, $V = (V_L + V_R)/2$. Steps in I_{CD} (dashed grey lines) correspond to single electrons populating the L/R sites (green/white circles label an electron presence/absence). The middle vertical shift (black dashed line) is a direct measure of the Coulomb repulsion between the neighbouring electrons (see text). **b**, Similar charge stability diagram to **a**, but with the polarizer nanotube positioned nearby (approximately 125-nm separation between the nanotubes). The interaction vertex is now horizontal, reflecting an attraction between the electrons. Along this line (dashed black) the ground state is degenerate between the two even states (0, 0) and (1, 1) ((n_L, n_R) represents the number of electrons in the L and R dots), whereas the odd states (1, 0) and (0, 1) are the excited states, separated by a pairing gap Δ from the ground state. This gap is maximal at the centre of the horizontal line, and its magnitude there is equal to the length of this line (2Δ when normalized to energy units; see Supplementary Information section S4). Note that the charge detector is far away from the right dot and that when the polarizer is close their mutual capacitance is strongly screened and so the charging lines of this dot are harder to observe. **c**, In the bare system, an electron populating the L site generates a Coulomb potential (green) that is positive (repulsive) in both the L and R sites. **d**, Embedding the system in a medium based on continuum electrostatics (purple) can at best screen the potential to zero far away from the electron, but cannot flip its sign. **e**, The key element for sign inversion is charge discreteness: a single-electron dipole (right) and a similarly shaped metal (left) will screen an external field differently (grey arrows). In the latter the internal field is nulled, whereas in the former it is larger and of opposite sign to the external field (red arrows; over-screening). This behaviour is rooted in the fact that an electron does not repel itself (see text). **f**, With a nearby polarizer, an electron charging the system gets dressed by the polarization (grey ellipse). The electrostatic potential (green) of the dressed particle will be substantially different to that of the bare electron (calculated in Supplementary Information section S4). Note that all the measurements presented here were done with single holes instead of single electrons, but to avoid unnecessary confusion we presented the physics in the language of electrons.

field, a single electron does not feel its own field and so can generate a large over-screening internal field, as long as this minimizes its single-particle energy.

To analyse the sign inversion microscopically, for the geometry of our system, we describe the polarizer by the Hamiltonian

$$H_{pol} = \frac{1}{2}\delta\hat{\sigma}_Z + t\hat{\sigma}_X \quad (1)$$

in which $\hat{\sigma}_Z = \psi_T^\dagger\psi_T - \psi_B^\dagger\psi_B$, $\hat{\sigma}_X = \psi_T^\dagger\psi_B + \psi_B^\dagger\psi_T$, $\psi_T^\dagger$ (ψ_T) and $\psi_B^\dagger$ (ψ_B) are creation (annihilation) operators of electrons in the two polarizer sites ('T', top; 'B', bottom), $\delta = \epsilon_T - \epsilon_B$ is the energy detuning between these sites, t is the tunnelling amplitude, and we ignored a constant energy offset. The repulsion between system and polarizer electrons leads to a charge–dipole coupling

$$H_{coup} = \frac{1}{2}U(n_L + n_R)(\hat{I} - \hat{\sigma}_Z) \quad (2)$$

in which n_L and n_R are the populations of the left and right system sites, U is the repulsion between an electron in one of these sites and an electron in the bottom site of the polarizer (assuming negligible interaction with the top site), and $\hat{I} = \psi_T^\dagger\psi_T + \psi_B^\dagger\psi_B$. This coupling dresses an electron entering the system with a dipolar excitation of the polarizer (Fig. 2f). In the strong coupling limit[5] ($U > t$, applicable to the measurements in Fig. 2b), the electron is dressed by a fully polarized dipole, and the effective potential of the dressed particle is considerably different from that of the bare electron (Supplementary Information section S4). If the charge–dipole coupling exceeds the charge–charge repulsion within the system

$$H_{repulsion} = Wn_Ln_R \quad (3)$$

that is, $U > W$, then the dressed potential at the neighbouring site has a flipped sign, implying that another electron is attracted to the dressed particle. This attraction reflects the fact that the neighbouring electron is more strongly attracted to the vacancy formed in the bottom site of

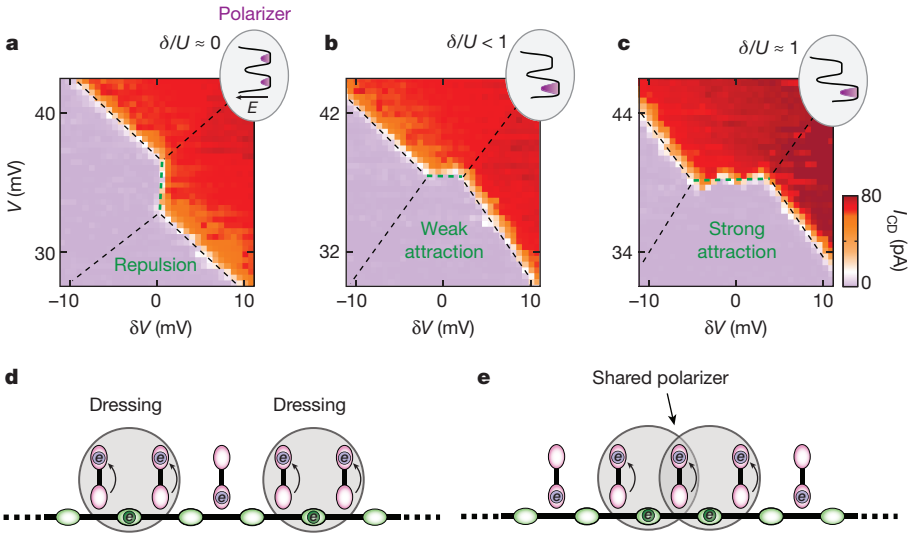

Figure 3 | Dependence of pairing energy on the polarizer detuning and the origin of the pair binding energy. a–c, Charge stability diagrams similar to those in Fig. 2b, measured for different energy detunings of the polarizer: $\delta = 0.39$ meV (**a**), 1.01 meV (**b**) and 2.57 meV (**c**). The observed attraction increases linearly with δ (more data in Supplementary Information section S6). The insets show the polarizer potential wells for the different detuning values. **d**, **e**, Rationalizing this observation using a toy model of the chain: two spatially separated electrons in the chain are each dressed by the polarization of their two adjacent polarizers (**d**); when the electrons are nearest neighbours, they share the centre polarizer and thus need to polarize one fewer polarizer (**e**). The energy gain, which gives the pairing energy, is consequently equal to δ, as we observe in the experiments in **a**–**c**. A similar polarizer-sharing argument holds for the two-site case, as is explained in Supplementary Information section S6.

the polarizer than it is repelled by the original electron that triggered the polarization.

A central prediction of the above model is a direct relationship between the emergent attraction and the underlying repulsion. We test this prediction by changing the separation between the nanotubes, which modifies the repulsion between system and polarizer electrons (U) while keeping the repulsion between the system electrons (W) fixed. The measured dependence of 2Δ on U (Supplementary Fig. 6) shows a linear dependence with unit slope. This result follows from equations (1)–(3) in the strong coupling limit (Supplementary Information section S4) and is a demonstration that the observed attraction is driven by repulsion.

Because the ability of the polarizer to dress an electron depends on its polarizability, one might expect that the optimal polarizer detuning for creating the strongest pairing would be at zero detuning ($\delta = 0$). At this detuning, the electronic wavefunction of the polarizer is symmetrically split between its top and bottom sites and its polarizability is maximal. However, the measured charge stability diagrams at different detunings (Fig. 3a–c) show that the attractive correction to the bare repulsion is not maximal at $\delta = 0$, but rather increases linearly with δ. This observation captures an important point about the origin of the pair binding energy, which is most easily rationalized by considering a toy model of a multisite chain (Fig. 3d, e): two far-apart electrons on the chain would each be dressed by two adjacent polarizers (Fig. 3d). In contrast, nearest-neighbour electrons share one polarizer and thus gain the polarization energy of one polarizer (Fig. 3e). This energy gain constitutes the pair binding energy, which is exactly equal to δ, the stored energy in a polarizer. This is indeed what we observe experimentally. The same mechanism of sharing the dressing costs, leading to a pairing energy of magnitude δ, also holds in our two-site case, as we explain in Supplementary Information section S6.

Beyond the ground-state stability diagram, we also examine whether pairing is reflected in transport, that is, whether electrons enter the system in pairs. In our set-up, we can measure the current through the polarizer and deduce the behaviour of the system via its strong correlations with the polarizer. To simplify the measurement, we open the barrier to one of the polarizer dots to strongly couple it to the lead, making the polarizer effectively a single quantum dot coupled to two leads (Fig. 4a). Now, the polarization is between dot and lead rather than between two dots. Although these two cases are electrostatically quite similar, they are fundamentally very different: whereas the excitonic polarization of an isolated double dot preserves the overall fermion parity of the combined system and polarizer, tunnelling of an electron to a lead in the polarizer does not. Yet, establishing pairing also in the latter configuration opens possibilities to create quantum systems with engineered dissipation, which may help to stabilize one-dimensional superconductivity[22].

Figure 4b shows the measured polarizer current, I_{pol}, with source–drain bias $V_{SD} = -1.3$ mV as a function of its local gate voltage, V_B, exhibiting a standard Coulomb blockade peak when the occupation of the polarizer dot is free to fluctuate. Owing to the strong coupling to the system, the peak position depends strongly on the electronic occupation of the system (Fig. 4b). If we fix V_B at 241.5 mV (dashed line in Fig. 4b), then the polarizer conducts for the odd system occupations (1, 0) and (0, 1), but is blocked for the even states. The Coulomb peak is pushed well below the Fermi energy for the (0, 0) state and well above it for the (1, 1) state. This behaviour persists throughout the charge stability diagram of the system (Fig. 4c, $V_{SD} = 100\,\mu$V), showing finite current (red) for odd states and negligible current (blue) for even states. Notably, the attraction survives even in the dynamic regime with tunnelling rates being a substantial fraction of the repulsion ($\Gamma_{pol}/U \approx 0.2$, $\Gamma_R/U \approx 0.45$ and $\Gamma_L/U \approx 0.23$, where $\Gamma_{L,R,pol}$ are the tunnelling rates to the left and right contacts of the system and to the polarizer contacts, respectively). Although neither the (0, 0) nor the (1, 1) states support single-particle current, we observe a finite current peak along their degeneracy line[23,24] (indicated by the arrow in Fig. 4c). Theoretical calculations (Fig. 4d) reproduce this peak only when including correlated many-body events in which an electron hopping in and out of the polarizer is accompanied by a pair of electrons simultaneously co-tunnelling out of and into the system (Supplementary Information section S7).

To better understand the processes underlying the observed current peak, we measure the current along a cut perpendicular to the degeneracy line, as a function of αV (where α, the independently measured lever-arm, normalizes V to energy units) and for varying V_{SD} (Fig. 4e). In different bias ranges we observe conductance regimes that differ in their turn-on slope, $s = dV_{SD}/d(\alpha V)$, which reflects the number of system electrons participating coherently in the dominant conductance

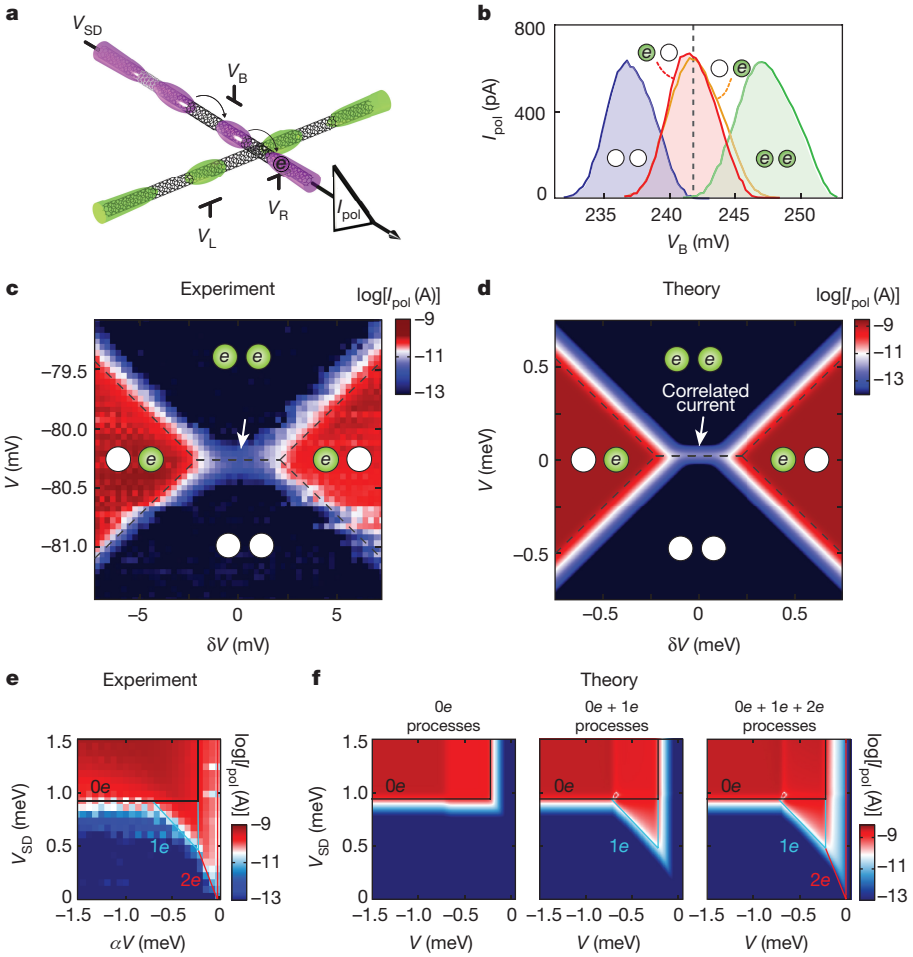

Figure 4 | Transport measurements. a, Experimental configuration. The polarizer current, I_{pol}, is measured with a finite bias on one lead, V_{SD}. The barrier between this lead and its nearby dot is reduced such that the dot becomes strongly connected to the lead, effectively making the polarizer nanotube a single quantum dot device with two leads. Compared to the experiments presented in Figs 2 and 3, in which the polarization occurred internally between two dots, here the polarization is between the dot and its lead. **b**, I_{pol} measured as a function of the local gate voltage, V_B, for four different population states of the system: blue, (0, 0); red, (1, 0); orange, (0, 1); green, (1, 1). In these measurements, the system charge remained fixed by staying far away from the charging lines of the system. This measurement was performed at a high bias, $V_{SD} = -1.3$ mV, which widens the observed charging lines. The vertical dashed line indicates the gate voltage V_B used in **c**. **c**, I_{pol} (colour scale) measured at $V_{SD} = 100\,\mu$V as a function of the voltage detuning between the L and R system sites, $\delta V = (V_L - V_R)/2$, and the mean voltage, $V = (V_L + V_R)/2$. Finite current (red) is observed for the odd system states, (1, 0) and (1, 0), and negligible current (blue) is measured for the even states, (0, 0) and (1, 1), except for a special peak of finite current (indicated by the white arrow) appearing along their degeneracy line. **d**, A theoretical master-equation calculation of I_{pol} for the parameters of the experiment (Supplementary Information section S7). The theoretical result features a finite current peak on the degeneracy line between the (0, 0) and (1, 1) states only when considering correlated processes that involve co-tunnelling of a pair of electrons into the system in concert with an electron tunnelling out of the polarizer. **e**, I_{pol} (colour scale) measured along a line cutting through the centre of the degeneracy line as a function αV and V_{SD} (the independently measured lever-arm, $\alpha = 0.61$, normalizes V to energy units). Three regimes appear at different bias ranges, differing in their turn-on slope, $s = dV_{SD}/(\alpha V)$, the value of which ($s \approx 0$, black line; $s \approx 1$, blue line; $s \approx 2$, red line) reflects the number of system electrons participating in the dominant transport process (0e, 1e or 2e, respectively) (see Supplementary Information section S7). **f**, Theoretical master-equation calculation of I_{pol} versus αV and V_{SD} with only a 0e system process considered (left), with $0e + 1e$ processes (middle) and with $0e + 1e + 2e$ processes (left). The 2e processes, which involve a pair tunnelling in the system, are the dominant processes at low bias, as is observed experimentally, although their calculated amplitude is lower than in the experiment, probably because the theory considers them to only the lowest order in tunnelling (Supplementary Information section S7).

process ($s = 0$, 1 and 2 corresponds to processes with zero, one and two system electrons, respectively). At high bias, $V_{SD} > 925\,\mu\text{eV} \approx U$, we observe $s \approx 0$ (Fig. 4e, black line), showing that a polarizer electron with enough energy to overcome its interaction with the system electrons (U) can flow without their cooperation. At intermediate bias, $V_{SD} > 490\,\mu$eV, the observed slope is $s \approx 1$ (Fig. 4e, blue line), reflecting simultaneous co-tunnelling of one system electron. Below this, and down to zero bias, the slope is $s \approx 2$ (Fig. 4e, red line), indicating that at low energies a pair of electrons co-tunnels into the system in concert with an electron tunnelling out of the polarizer. Theoretical calculations (Fig. 4f and Supplementary Information section S7) reproduce the main features, although they give a smaller two-electron current than is observed experimentally, probably because they consider these processes to only the lowest order in tunnelling.

Our work experimentally establishes the fundamental concept of excitonic pairing of electrons that was theorized half a century ago. The ability to construct the basic building block of electronic attraction raises many questions regarding the possibility of engineering exotic states of matter by generalizing this concept to larger systems, for example, whether it would be possible to create an artificial superconductor, what kind of pairing such a superconductor would have, and whether it would be stable against competing ground states (see Supplementary Information section S8 for further discussion). The benefit of repulsion-driven attraction is that the pairing energy of the

attraction increases linearly with decreasing device dimensions. Our experiments achieved pairing energies of about 8 K with rather large quantum dots (approximately 400 nm). By extrapolating this value to the nanometre scale, we postulate that it should be possible to reach energies well in excess of room temperature. Given the tremendous progress in engineering quantum dots in two-dimensional semiconductors[25–28], down to almost single-atom scale[29], the possibilities to engineer interesting states of matter based on electronic attraction now seem very promising.

Received 17 January; accepted 26 May 2016.

1. Little, W. A. Possibility of synthesizing an organic superconductor. *Phys. Rev.* **134,** A1416–A1424 (1964).
2. Ginzburg, V. L. Concerning surface superconductivity. *Sov. Phys. JETP* **20,** 1549–1550 (1964).
3. Allender, D. & Bardeen, J. Model for an exciton mechanism of superconductivity. *Phys. Rev. B* **7,** 1020–1029 (1973).
4. Ginzburg, V. L. High-temperature superconductivity—dream or reality? *Sov. Phys. Usp.* **19,** 174–179 (1976).
5. Hirsch, J. E. & Scalapino, D. J. Excitonic mechanism for superconductivity in a quasi-one-dimensional system. *Phys. Rev. B* **32,** 117–134 (1985).
6. Micnas, R., Ranninger, J. & Robaszkiewicz, S. Superconductivity in narrow-band systems with local nonretarded attractive interactions. *Rev. Mod. Phys.* **62,** 113–171 (1990).
7. Jérome, D. in *The Physics of Organic Superconductors and Conductors* (ed. Lebed, A.) 3–16 (Springer, 2008).
8. Raikh, M. E., Glazman, L. I. & Zhukov, L. E. Two-electron state in a disordered 2D island: pairing caused by the coulomb repulsion. *Phys. Rev. Lett.* **77,** 1354–1357 (1996).
9. Bardeen, J., Cooper, L. & Schrieffer, J. Microscopic theory of superconductivity. *Phys. Rev.* **106,** 162–164 (1957).
10. Hirsch, J. E. & Scalapino, D. J. Double-valence-fluctuating molecules and superconductivity. *Phys. Rev. B* **32,** 5639–5643 (1985).
11. Varma, C. Missing valence states, diamagnetic insulators, and superconductors. *Phys. Rev. Lett.* **61,** 2713–2716 (1988).
12. Matsushita, Y., Bluhm, H., Geballe, T. H. & Fisher, I. R. Evidence for charge Kondo effect in superconducting Tl-doped PbTe. *Phys. Rev. Lett.* **94,** 157002 (2005).
13. Butler, M. R., Movaghar, B., Marks, T. J. & Ratner, M. A. Electron pairing in designer materials: a novel strategy for a negative effective Hubbard U. *Nano Lett.* **15,** 1597–1602 (2015).
14. Oganesyan, V., Kivelson, S., Geballe, T. & Moyzhes, B. Josephson tunneling spectroscopy of negative-U centers. *Phys. Rev. B* **65,** 172504 (2002).
15. Hirsch, J. E., Tang, S., Loh, E. Jr & Scalapino, D. J. Pairing interaction in two-dimensional CuO_2. *Phys. Rev. Lett.* **60,** 1668–1671 (1988).
16. Ge, J. *et al.* Superconductivity above 100 K in single-layer FeSe films on doped $SrTiO_3$. *Nat. Mater.* **14,** 285–289 (2015).
17. Richter, C. *et al.* Interface superconductor with gap behaviour like a high-temperature superconductor. *Nature* **502,** 528–531 (2013).
18. Cheng, G. *et al.* Electron pairing without superconductivity. *Nature* **521,** 196–199 (2015).
19. Firstenberg, O. *et al.* Attractive photons in a quantum nonlinear medium. *Nature* **502,** 71–75 (2013).
20. Waissman, J. *et al.* Realization of pristine and locally tunable one-dimensional electron systems in carbon nanotubes. *Nat. Nanotechnol.* **8,** 569–574 (2013).
21. Averin, D. V. & Bruder, C. Variable electrostatic transformer: controllable coupling of two charge qubits. *Phys. Rev. Lett.* **91,** 057003 (2003).
22. Lobos, A. M., Iucci, A., Müller, M. & Giamarchi, T. Dissipation-driven phase transitions in superconducting wires. *Phys. Rev. B* **80,** 214515 (2009).
23. Goldstein, M., Berkovits, R. & Gefen, Y. Population switching and charge sensing in quantum dots: a case for a quantum phase transition. *Phys. Rev. Lett.* **104,** 226805 (2010).
24. Yoo, G., Park, J., Lee, S.-S. B. & Sim, H.-S. Anisotropic charge Kondo effect in a triple quantum dot. *Phys. Rev. Lett.* **113,** 236601 (2014).
25. Medford, J. *et al.* Quantum-dot-based resonant exchange qubit. *Phys. Rev. Lett.* **111,** 050501 (2013).
26. Braakman, F., Barthelemy, P., Reichl, C., Wegscheider, W. & Vandersypen, L. M. K. Long-distance coherent coupling in a quantum dot array. *Nat. Nanotechnol.* **8,** 432–437 (2013).
27. Seo, M. *et al.* Charge frustration in a triangular triple quantum dot. *Phys. Rev. Lett.* **110,** 046803 (2013).
28. Delbecq, M. R. *et al.* Full control of quadruple quantum dot circuit charge states in the single electron regime. *Appl. Phys. Lett.* **104,** 183111 (2014).
29. Fölsch, S., Martínez-Blanco, J., Yang, J., Kanisawa, K. & Erwin, S. C. Quantum dots with single-atom precision. *Nat. Nanotechnol.* **9,** 505–508 (2014).

Supplementary Information is available in the online version of the paper.

Acknowledgements We thank E. Altman, E. Berg, Y. Gefen, M. Goldstein, U. Leonhardt, G. Refael and A. Yacoby for discussions and D. Mahalu for the e-beam writing. K.K. acknowledges support from the Carlsberg Foundation. Y.O. acknowledges support by Minerva, BSF and ERC Adg grant (FP7/2007-2013 340210). F.v.O. acknowledges support through SPP 1459 and SFB 658. S.I. acknowledges financial support by the ERC Cog grant (See-1D-Qmatter, No. 647413).

Author Contributions A.H., A.B., I.S. and S.I. performed the experiments, analysed the data, contributed to its theoretical interpretation and wrote the paper. I.S. built the scanning probe microscope. I.K. built the custom measurement instrumentation for the experiment. J.W. designed and fabricated the devices. K.K., Y.O. and F.v.O. developed the theoretical model. K.K. performed the theoretical simulations.

Author Information Reprints and permissions information is available at www.nature.com/reprints. The authors declare no competing financial interests. Readers are welcome to comment on the online version of the paper. Correspondence and requests for materials should be addressed to S.I. (shahal.ilani@weizmann.ac.il).

Reviewer Information *Nature* thanks R. Egger, T. Kontos and E. Scheer for their contribution to the peer review of this work.